This is a non-peer reviewed preprint that has been submitted for publication in Journal of the Geological Society.

Evolution of a shear zone before, during and after melting

Amicia L Lee[1]*, Geoffrey E Lloyd[1], Taija Torvela[1] & Andrew M Walker[1]

[1]*School of Earth and Environment, University of Leeds, UK*

**Corresponding author (e-mail:earall@leeds.ac.uk)*

Abstract: Partial melt in the deforming mid/lower continental crust causes a strength decrease and drives formation of lithological heterogeneities. However, mechanisms of formation of syn-melt deformation zones and strain partitioning in partially molten rock remain poorly understood. We use field and microstructural observations to unravel the evolution of a syn-melt shear zone, Seiland Igneous Province, Northern Norway. The paragneiss shear zone, part of a series within intruded gabbros, formed by syn-intrusive deep crustal shearing during lithospheric extension relating to Iapetus Ocean opening. Strain localisation is primarily controlled by partial melt and subsequent grain size heterogeneities. Pre-melt microstructures indicate initial deformation at high temperatures and low stresses, resulting in solid state, static grain growth. During melting, melt migrates towards the shear zone centre, where strain localises. Crystallisation promotes further grain growth and a 'strong' centre relative to finer grained, weaker shear zone margins, where subsequent deformation localises forming large scale 'paired shear zones'. Melt textures are absent at shear zone margins and microstructures indicate deformation at lower temperatures and higher stresses. In effect, melt migration towards the shear zone centre ultimately led to strengthening of the shear zone core, with post-crystallisation deformation focusing along shear zone margins where significant heterogeneities are present.

Experimental studies of partially molten rock show there is dramatic strength drop when partial melt forms a connected network at $\sim$7% melt volume (e.g. Rosenberg and Handy, 2005). This strength decrease is propagated as melt volume increases and deformation partitions between the solid rock and liquid melt (Vanderhaeghe, 2009). Partial melting is common in the middle to lower continental crust due to high temperatures, decompression and/or the influence of volatiles promoting pervasive melting (Sawyer, 1994; Brown, 2001; Vanderhaeghe, 2009). Partial melt adds to the heterogeneous nature of these rocks (e.g. grain size, mineralogy, microstructure, etc.), and such lithological heterogeneities are important factors in controlling strain partitioning on all scales (Fossen and Cavalcante, 2017). Rheological relationships have been well constrained from experiments; however, experiments do not always explain observed partial melt at outcrop scale in the field or crustal scale from the geophysical response (Brown et al., 1995; Rosenberg and Handy, 2005; Karato, 2010; Lee et al., 2017). For example, if melt localises strain, it is unclear why very large volumes of melt remain in-situ within the crust (crystallising in the form of migmatites), despite their sometimes immediate proximity to one or several shear zones that should act as conduits for melt escape (Labrousse et al., 2004; Lee et al., 2018).

It is important to consider how shear zones evolve through time and what role partial melt plays in their evolution. The active deformation mechanisms and strain localisation in partial melt shear zones vary during their evolution from phases of melt-free to syn-melt and post-melt deformation. Strain localisation is influenced by many parameters within shear zones; for example, pre-existing fractures, weak layers or structures (Passchier, 1982; Austrheim and Boundy, 1994; Pennacchioni and Cesare, 1997), margins of a lithological heterogeneity such as paired shear zones (Pennacchioni and Mancktelow, 2007) and thickness change(s) through time (Hull, 1988; Means, 1995; Vitale and Mazzoli, 2008).

The actively deforming area and overall thickness of shear zones can vary during shear zone development and is summarised by Fossen and Cavalcante (2017). Generally, shear zones with a small offset and length are thinner than shear zones with larger offset and longer length. This behaviour suggests that as a shear zone grows and the offset increases, the shear zone must also increase in thickness, potentially contradicting the assumption that shear zones strain soften as strain accumulates (Fossen and Cavalcante, 2017). Many theoretical models have been proposed for the evolution of shear zone thickness (e.g. Hull, 1988; Means, 1995; Vitale and Mazzoli, 2008). Two of these models are summarised as follows: 'Type 1' shear zones thicken over time as strain propagates into the walls, leaving an inactive central part behind;

and ‘Type 2’ shear zones form as strain increasingly localises to the central part of the shear zone.

In this paper, we investigate the microstructural signature of a syn-kinematic partial melt shear zone from the Øksfjord peninsula in the Seiland Igneous Province (SIP) of the North Norwegian Caledonides. Deformation of the shear zone occurred at the same time as biotite dehydration melting and granulite facies metamorphism, where the intrusion of large gabbroic plutons at the base of the lower crust provided the heat source for the high temperature metamorphism and partial melting (Elvevold et al., 1994; Menegon et al., 2011). Identification of phases of pre-, syn- and post-melt deformation make the Øksfjord shear zone an ideal system to study the processes and effects of partially molten lower crustal deformation.

Geological setting

The SIP (Figure 1a) comprises of a suite of deep-seated, rift-related, mantle-derived magmatic rocks emplaced into paragneisses during the opening of the Iapetus Ocean at 570-520 Ma (Elvevold et al., 1994; Reginiussen et al., 1995; Roberts et al., 2006). It forms part of the Sørøy Nappe of the Kalak Nappe complex, which is the middle allochthon of the Norwegian Caledonides. The Sørøy Nappe comprises paragneiss of the Sørøy Group estimated at between 1.7-1.2 Ga in age (Robins and Often, 1996). The lowest stratigraphic unit of the Sørøy Nappe is the Eidvågeid Supracrustal Sequence, a paragneiss comprising migmatized pelitic and quartzofeldspathic gneisses, quartzite, marble and calc-silicate rocks (Akselsen, 1982). There is little evidence for the origin of the Eidvågeid Supracrustal Sequence; it is not known whether it is previously deformed basement or the lowest part of the stratigraphic sequence of the Sørøy Group. The structurally overlying Sørøy Group consists of meta-psammites, schists, marble and calc-silicates recording a transition from shallow water clastic deposition to turbidite-type sedimentation (Roberts, 1974; Ramsay et al., 1985).

During the late Proterozoic (829-804 Ma) the Sørøy Group was deformed and metamorphosed. This was followed by intracontinental rifting, similar to the current East African Rift, where magmatic rocks ranging in composition from ultrabasic to nepheline syenitic and carbonatitic were emplaced into continental crust of the allochthonous Kalak Nappe (Ramsay et al., 1985; Krogh and Elvevold, 1990; Elvevold et al., 1994; Roberts, 2003; Roberts et al., 2006). The intrusive event was short-lived, between 570-560 Ma, and emplaced during a pre-orogenic extensional phase related to the initial stages of the opening of the Iapetus

Ocean (Reginiussen et al., 1995; Roberts et al., 2006). The total extent of magmatism is unknown but was much more voluminous than the current surface exposure of 5400 km^2, which only represents the roots of the intrusions (Roberts et al., 2006). A further phase of deformation and medium to high grade metamorphism was caused by the Finnmarkian Orogeny between 530-490 Ma, an early phase of the Caledonian Orogeny (Sturt et al., 1978; Ramsay et al., 1985; Ramsay and Sturt, 1986; Robins and Often, 1996). This was followed by the thrusting of nappes during the Scandian Orogeny between 420-400 Ga, a later phase of the Caledonian Orogeny (Stephens and Gee, 1989).

[Figure 1 about here.]

The Øksfjord peninsula (Figure 1b) consists almost entirely of layered gabbro plutons intruded into paragneiss and metapelites of the Eidvågeid Sequence, which now outcrop c. 50 km northeast of Øksfjord in the Kalak Nappe Complex (Akselsen, 1982; Elvevold et al., 1994; Reginiussen et al., 1995). During the intrusive event, the Eidvågeid gneisses suffered contact metamorphism to peak conditions of T = 930-960°C and P = 0.55-0.7 GPa before cooling and recrystallising at pyroxene granulite facies conditions (700-750°C, 0.5-0.7 GPa; Elvevold et al., 1994). A steeply dipping (∼60° WSW) gneissic to mylonite foliation developed in the metasediments and gabbro during this period of metamorphism, with asymmetric fabrics indicating a top-down-to-NW sense of shear (Menegon et al., 2011). The relationship of magmatic layering with the paragneiss foliation suggests synintrusive deep crustal shearing during lithospheric extension (Elvevold et al., 1994; Roberts et al., 2006). The study area focusses on a 2 km section through a laterally continuous paragneiss Øksfjord shear zone (ØSZ) on the Øksfjord Peninsula. This shear zone can be traced northward to outcrops on the edge of Økfjorden (Figure 1 b-c).

According to thermodynamic modelling the paragneiss and metapelites have undergone shearing and partial melting at metamorphic conditions of T = 760-820°C and P = 0.75-0.95 GPa (Menegon et al., 2011) via biotite dehydration (bt + pl + sil + qz = kf + gt + melt; Spear et al., 1999). The paragneiss is segregated into leucosome- and melanosome-rich domains visible from outcrop to microscale. It is estimated 5-7% melt was produced during partial melting and shear deformation (Menegon et al., 2011).

Field observations

The boundary of the paragneiss ØSZ is not distinct, there is a transition from gabbro to paragneiss ‘pods’ hosted in gabbro to paragneiss ØSZ (Figure 1c). The dominant lithology in the transition zone is foliated gabbro. The paragneiss ‘pods’ are also foliated, showing stromatic layering with clear mineral segregation. However, this transition is not a simple linear increase of migmatized paragneiss compared to gabbro. Figure 2 shows representative outcrop photographs through this transition and into the centre of the ØSZ. Sample SIP09 is a gabbro in which the foliation is indistinct (Figure 2a); it marks the edge of the transition zone from where paragneiss is present. Figure 2b shows an example of the paragneiss texture where it is surrounded by gabbro. These zones are typically up to 10 to 50 m in size, although they are more common closer to the main ØSZ. The paragneiss exhibits a N-S trending gneissic to mylonitic foliation with a stretching lineation plunging moderately towards the NW. This foliation is parallel to the primary magmatic layering preserved in some areas of the gabbro (Elvevold et al., 1994; Roberts et al., 2006).

[Figure 2 about here.]

Within the ØSZ the rocks have a higher felsic content within a garnet-granulite mineral assemblage. Figure 2 c-i show typical outcrop exposures observed in the ØSZ. From the field it is difficult to determine exact areas of melt within the paragneiss; however, the presence of a high temperature mineral assemblage, more than one type of migmatite texture, and larger ‘pools’ of leucosome allow us to infer that the system was melt bearing. The paragneiss typically displays stromatic migmatite textures, with layering observed on a variety of scales (Figure 2 d-h). The stromatic layering of the migmatite shows the segregation of the leucosome (felsic) and melanosome (mafic) stroma of various thicknesses from the millimetre to decimetre scale. SIP15, located just inside the ØSZ boundary, is a schollen-type migmatite where rafts of non-migmatized restite remain intact and the leucosome flows around the rafts (Figure 2c). The centre of the paragneiss ØSZ has linear stroma, although in some places tight parasitic folds deform the stromatic migmatite. Layer thickness remains constant in most folded migmatites (Figure 2f), but in some localities the leucosome varies in thickness and the fold hinges in the restite have thickened to form similar folds. Where present, kinematic indicators in the paragneiss show normal offset shearing top down to both east and west, although top down to the west is more common and suggests oblique sinistral-normal displacement due to shearing (Figure 2 h-i).

Microstructural analysis

As some of the leucosome can segregate through solid state processes as opposed to melting, it is important to consider the microstructure to understand melting processes and volumes. Melting occurred by biotite dehydration, where K-feldspar, garnet and melt are products of the reaction: bt + qz + pl + sil = melt + gt + kf (Figure 3; Spear et al., 1999; Menegon et al., 2011). The melt predominantly crystallises as K-feldspar, plagioclase and ilmenite (Figure 3).

[Figure 3 about here.]

Grain boundary melt is very common in the ØSZ samples and is generally composed of K-feldspar, plagioclase and ilmenite (Figure 3). Reaction textures of plagioclase and biotite are observed to breakdown to form K-feldspar, with ilmenite infilling nearby pore space (Figure 3). In addition to grain boundary melting, 'melt zones' are also observed in SIP11 located outside the main shear zone. Complex melt-rock interaction textures are observed where cordierite and orthopyroxene are replaced by biotite, sillimanite and ilmenite (Figure 3e). Orthopyroxene is a major phase in samples located in the transition zone from gabbro to paragneiss; within the shear zone it is either not present or a minor phase. The lack of orthopyroxene within the paragneiss shear zone suggests the transition area may be of a different composition and/or origin to the shear zone.

The melt-solid-solid dihedral angle in the paragneiss ranges from 4° to 85° with a median of 26°, mean of 29° and standard deviation of 17° (method after Holness and Sawyer, 2008). When the low dihedral angle is considered alongside the abundant presence of grain boundary melt films, it appears that melt connectivity was high in the ØSZ. The solid-solid-solid dihedral angles from ØSZ paragneisses are not in solid-state equilibrium as grain boundary dihedral angles vary from 49° to 179° with a median of 110°, mean of 109° and standard deviation of 31°. The large range of dihedral angles is the result of deformation microstructures forming sutured grain boundaries.

Crystallised melt volume is calculated from microstructural and image analysis. The quantification is for the melt textures that remain in the microstructure; therefore, it could be an underestimate if significant melt loss/escape has occurred or an overestimate if melt crystallised in the shear zone during multiple melt fluxes. Preserved melt textures suggest a peak crystallised melt volume for SIP20 of $<$15% and 10-15% for nearby samples SIP 18, 19, 21 and 23. Towards the edges of the shear zone melt textures are poorly preserved where <5% crystallised melt is observed for samples SIP 16, 17, 24 and 43.

Quartz is usually present as large grains or recrystallised ribbons; it is not present as a melt or reactive phase in areas where melt-rock reactions are observed (e.g. Figures 3 c-e). As quartz is not considered a primary crystallised product of biotite dehydration melting, it is inferred that quartz preserves a deformation history from the ØSZ. During melting, strain localises into the melt, but if shearing is also active after crystallisation, the peritectic phases may show evidence of deformation and melt textures may be destroyed.

[Figure 4 about here.]

Towards the centre of the ØSZ it is typical to observe chessboard subgrain extinction in large quartz grains (>800 μm; Figure 4b), often accompanied by an undulose extinction overprint. Where the grain size is smaller (50-200 μm; Figure 4 a-b), quartz exhibits a lobate microstructure with serrated grain boundaries typical of grain boundary migration (GBM) microstructures. Here, rapid grain boundary mobility is favoured by high temperatures, sweeping through grains and removing dislocations (Guillope and Poirier, 1979; Urai et al., 1986; Hirth and Tullis, 1992; Stipp et al., 2002). Figure 4a shows a central band where there is evidence for melt reactions in the pressure shadows of plagioclase. This 'melt zone' is cutting quartz zones exhibiting GBM-type recrystallisation. The quartz-plagioclase grain boundaries are straight and preservation of melt next to deformation microstructures suggests the GBM quartz deformation predates melting. The presence of chessboard extinction and GBM suggests the quartz deformed at high temperatures and mid to low stresses (Kruhl, 1996). The undulose extinction overprint suggests minor retrograde deformation at lower temperatures (Figure 4b).

Grain size decreases towards the edges of the ØSZ (10-80 μm). Here, quartz grains have broken down to subgrains and dynamically recrystallised neoblasts; characteristic of subgrain rotation (SGR) recrystallisation where additional dislocations allow the rotation of subgrains to develop new grains (Figure 4 d-e Hirth and Tullis, 1992; Stipp et al., 2002). Figure 4a shows evidence of a non-deformation textural relationships between melt and the deformed quartz; in contrast, Figure 4 c-d shows that the melt reacting phases (fine grained biotite and k-feldspar) have been sheared and entrained during the formation of the SGR quartz ribbons and shearing of larger sigmoidal K-feldspar clasts. This suggests deformation of quartz at the edges of the ØSZ was active at lower temperatures and higher stresses than the centre of the ØSZ (Hirth and Tullis, 1992; Stipp et al., 2002). Post-crystallisation deformation lead to poor preservation of melt textures in quartz dominant zones. Large K-feldspar grains in these samples are winged mantled σ-type clasts with a sinistral sense of shear. A peritectic texture is expected to be produced from melting but the peritectic phases are deformed with grain mantles at the edges of the shear zone suggesting post-melt deformation.

Garnet is a peritectic product of biotite dehydration melting. Euhedral garnet grains, 200 to 500 μm in size, are preserved in the centre of the ØSZ (Figure 3f). Garnet grains towards the edges of the ØSZ are retrogressed, breaking down to quartz, K-feldspar, plagioclase and biotite (Figure 4f). Instead of the large peritectic garnets observed in the centre, the garnets are 50 to 200 μm with irregular grain shapes. Deformation at the edges of the ØSZ is likely to have occurred post melting as melt microstructures are not preserved and peritectic phases are deformed.

Crystallographic preferred orientations

The crystallographic preferred orientations (CPO) for quartz-bearing samples within the ØSZ were analysed using the FEI Quanta 650 FEGSEM equipped with AZtec software and an Oxford/HKL Nordlys S EBSD system at the University of Leeds. All samples were run with a 20 kV accelerating voltage, 5 μm spot size and 5 μm step size; the maximum step size is constrained by the minimum grain size (20 μm); using the same step size ensures consistency when calculating grain and subgrain relationships.

[Figure 5 about here.]

Figure 5 shows the quartz pole figures for ten samples from within the ØSZ. Samples SIP 16, 17, 24 and 43 show similar CPOs with an X-Y girdle in <a> and a maximum at Z in [c]. There is a slight asymmetry, especially in SIP17 where the [c] maxima suggests a sinistral shear component, compatible with field evidence. The CPO in these samples suggests deformation by basal <a> slip (e.g. Law et al., 1990). Samples SIP 20 and 19 in the centre of the ØSZ have a [c] maxima parallel to the Y direction, compatible with prism <a> slip in quartz (e.g. Law et al., 1990). Samples between edges and centre of the ØSZ (SIP 18, 21, 22) have weak CPO's with diffuse poles at Z in [c]. When the weak CPO is considered against their geographic position in the ØSZ, it is suggested that the crystal fabric represents an evolution through fabric overprinting from prism <a> slip in the centre and basal <a> slip at the edges (especially samples SIP18 and 21). SIP15, located at the edge of the ØSZ, is anomalous and shows a similar CPO to SIP20. This sample has large quartz grains with chessboard extinction and GBM in the smaller grains; it also correlates to a secondary peak in leucosome/melt fraction.

Stress and strain rate estimates

Deformation mechanisms and CPO analysis provide qualitative data for stress and strain, whilst palaeopiezometery allows quantification of differential stress from grain size (e.g. Twiss, 1977; Ord and Christie, 1984; Stipp and Tullis, 2003; Cross et al., 2017). It is possible therefore to estimate strain rate via flow laws (e.g. Luan and Paterson, 1992; Gleason and Tullis, 1995; Hirth et al., 2001). Generally, the smaller the recrystallised grain size, the higher the differential stress. However, in a melt present system, grains crystallising from the melt are typically larger than grains of the same mineral deformed in solid state. Thus, palaeopiezometers can only be used to quantify deformation post-melting. The results shown here give the relative change in magnitude of stress and strain rate across the ØSZ.

[Figure 6 about here.]

The centre of the shear zone has the highest palaeomelt content, which is problematic for calculation of stress from grain size. At the edges of the shear zone, our interpretation is that SGR deformation and basal <a> slip were active post-crystallisation. It is appropriate therefore to apply a palaeopiezometer here. The recrystallised grain size is calculated from EBSD data via the grain orientation spread technique after Cross et al. (2017), whereby recrystallised and relict grains are isolated to find the recrystallised grain size (Figure 6). The Cross et al. (2017) piezometer relationship is applied to calculate the differential stress (σ_{1-3}) from recrystallised grain size (D) for quartz bearing samples in the ØSZ,

$$D = 10^{3.91\pm0.51}\sigma_{1-3}^{-1.41\pm0.21}. \tag{1}$$

Figure 6 shows the variation in recrystallised grain size across the ØSZ. The grain size relationship loosely follows the melt volume trend; both increase towards the centre of the shear zone (e.g. root mean squared recrystallised grain size in the centre is 48.2 $\pm$ 7.6 μm, SIP 19, 20, and drops to 21.6 $\pm$ 10.2 μm at the edges, SIP 16, 17, 24, 43). The grain size relationship corresponds to samples where GBM is dominant (large, centre) and samples where SGR is active (small, edges).

The palaeopiezometer is applied to the rms recrystallised grain sizes to calculate the differential stresses (Figure 6). The differential stress in the centre of the shear zone is 38 $\pm$ 4.3 MPa (SIP 15, 19, 20), increases to 41 ± 11.5 MPa with the evolving quartz fabric (transition from prism <a> to basal <a> slip; SIP 18, 21, 22) and further increases to 68 ± 17 MPa for the shear zone edges (SIP 16, 17, 24, 43). The differential stress variation within the shear zone therefore suggests faster strain rates at the edges of the shear zone and slower strain rates in the centre.

The rheological behaviour of rocks is expressed through flow laws, which describe the dependence of strain rate on parameters such as stress and temperature (Poirier, 1985; Hirth et al., 2001). In this paper we apply the quartz power-law flow law for dislocation creep (Tokle et al., 2019) to understand any relative changes in magnitude of strain rate,

$$\dot{\varepsilon} = A\sigma_{1-3}^{n} f_{\mathrm{H_2O}}^{r} e^{\frac{-Q}{RT}}, \tag{2}$$

where $\dot{\varepsilon}$ is strain rate, σ_{1-3} is differential stress, n is the stress exponent, $f_{\mathrm{H_2O}}$ is the water fugacity, r is the water fugacity exponent, Q is the activation enthalpy, R is the ideal gas constant, T is absolute temperature, and A is a material parameter. The flow law parameters for dislocation grain boundary sliding with a power-law stress exponent of n = 4 are: Q = 125 kJ/mol, r = 1, $f_{\mathrm{H_2O}}$ = 200 MPa, and A = 1.75×10^{-12} MPa^{-n}; and parameters for low temperature/high stress dislocation creep with a stress exponent of n = 3 are: Q = 115 kJ/mol, r = 1.2, $f_{\mathrm{H_2O}}$ = 50 MPa, and A = 1.1×10^{-12} MPa^{-n}/s, where the final strain rate is the sum of the dislocation grain boundary sliding component and the dislocation creep component. If the quartz power-law flow law for dislocation creep is applied to the calculated stresses, it yields strain rates of 4.6×10^{-12}, 3.7×10^{-12} and 2.8×10^{-11} for the ØSZ centre, transitioning fabric and edges respectively. Whilst these estimates do not represent the true deformation conditions of the ØSZ, they do indicate that the shear zone edges deformed at an order of magnitude faster strain rate than the shear zone centre during post-crystallisation deformation.

Discussion

The ØSZ is a high strain deformation zone of migmatized paragneiss, which transitions to foliated gabbro with pockets of paragneiss to foliated gabbro with no evidence for partial melting. It is part of a series of thin ductile paragneiss shear zones within the gabbro that formed by synintrusive deep crustal shearing during lithospheric extension (Elvevold et al., 1994; Roberts et al., 2006). The paragneiss is strongly sheared and kinematic indicators suggest oblique sinistral-normal faulting, supporting the extensional rifting model for the SIP (Reginiussen et al., 1995). The pockets of paragneiss in the gabbro are richer in orthopyroxene than samples in the main shear zone, suggesting a different protolith. During the percolation of melt through the system, it is possible that the melt infiltrated into the gabbro wall rock and the paragneiss pods could be the result of metasomatism of the gabbro.

Typically palaeo shear zones have a grain size distribution of coarse grains at the edges and fine grains in the centre where the strain was higher (Figure 7a; Ramsay and Graham, 1970; White, 1979; Olgaard and Evans, 1988). In the ØSZ the reverse is the case, with large grains in the centre and small grains at the edges (Figure 6). The normal grain size distribution is only observed in melt-free areas. It seems therefore that the inverse grain size distribution in the ØSZ is the result of the influence of melt in the system. Grain growth is promoted at high temperatures and transport of melt through the system, which can occur in two ways: static recrystallisation outpacing dynamic recrystallisation (Evans et al., 2001), or crystallisation of grains directly from melt where crystallisation rate outpaces strain rate (Jurewicz and Watson, 1985). In the ØSZ it is likely that both processes were active, resulting in grain growth of solid and peritectic phases. The melt textures present indicate up to 15% melt crystallised in-situ in the centre of the system, decreasing in volume through to the edges of the ØSZ and within the transition zone. This does not suggest 15% melt was present at any one time but does suggest melt may have pooled and crystallised if unable to escape the system. Higher melt volumes may have been present at the shear zone edges but it may have been transported to the centre or completely escaped the shear zone. Grain growth is greater in the centre of the ØSZ as a result of the enhanced crystallised melt presence here.

Menegon et al. (2011) suggested 5-7% melt was located in isolated pockets and did not control the mechanical strength of the ØSZ. However, in the shear zone samples studied here, located $\sim$10 km south of those sampled by Menegon et al. (2011), melt has low dihedral angles and forms grain boundary melt films forming an interconnected melt framework. Interconnected melt networks result in mechanical weakening during melting; the 5-7% melt present in the ØSZ is sufficient to cause a dramatic strength decrease and thus control the mechanical strength of the shear zone (Figure 7b; Rosenberg and Handy, 2005; Llorens et al., 2019). Degli Alessandrini et al. (2017) analysed dry mafic dykes from the same area as Menegon et al. (2011) and suggested that melt-induced chemical reactions may be a common feature in the lower crust and responsible for weakening the dry, strong mafic rocks. As a result melt-assisted deformation in the lower crust is likely to have a dramatic effect on the strength of dry, strong mafic rocks.

The deformation phase that formed the GBM-type fabric in the centre of the ØSZ is likely to have occurred pre-melting as little deformation is observed in the peritectic melt phases and melt microstructures are well preserved and cut zones of deformed quartz (Figures 4a, 7 a, b). At the edges of the ØSZ, the quartz grain size has been reduced due to SGR. When this grain size reduction is considered alongside deformed feldspar grains, lack of chessboard extinction, entrained peritectic minerals in quartz ribbons and lack of peritectic garnet, it supports our contention that the edges of the ØSZ deformed post-melting at higher stresses and lower temperatures (Figure 7c).

From microstructural and CPO analysis, there were two deformation phases active in the ØSZ; (1) high-temperature deformation (GBM and prism <a> slip) observed in the centre of the shear zone; and (2) mid-temperature deformation (SGR and basal <a> slip) observed at the edges. The slip systems and deformation mechanisms responsible for the recorded CPOs and microstructure in the ØSZ are likely to have been active at different times as a steep temperature gradient over the narrow shear zone is unlikely. This is supported by evidence of deformation microstructures overprinting melt microstructures at the edges of the ØSZ (Figures 4d, 7c), suggesting the edges deformed later than the centre.

[Figure 7 about here.]

During prograde metamorphism before melting, quartz begins to deform by GBM and prism <a> slip (Figure 7a). Experiments suggest GBM and prism <a> slip is favoured by high temperature and low stress deformation (Nachlas and Hirth, 2015; Richter et al., 2016). Partial melting in the ØSZ occurred at high temperatures (760-820°C; Menegon et al., 2011) and during this evolution phase, stress was absorbed by the melt (Figure 7b). Percolation of partial melt through the shear zone resulted in an overprinting of the GBM deformation microstructure by melt textures (Figure 7b).

Upon crystallisation of the system and subsequent cooling, there is no melt to localise strain (Brown, 2001,0; Yakymchuk and Brown, 2014). Where melt crystallises, the rock is strengthened as pre-existing dislocations will have been removed during the recovery process of GBM recrystallisation, as well as the relative grain size increase during crystallisation (Walte et al., 2003,0; Otani and Wallis, 2006). Subsequent post-melt deformation is localised to the finer-grained edges of the ØSZ as it is easier to deform finer grains by diffusion-accommodated grain boundary sliding and diffusion creep than coarser grains (Figure 7c;

Karato et al., 1986; Nixon et al., 1992). This produces the SGR microstructures and basal <a> slip CPO observed at the ØSZ edges where deformation occurs at lower temperatures and higher stresses than GBM.

Microstructures from the ØSZ show evidence for different deformation conditions. The first phase was active pre-melt and involved deformation at high temperatures. This was followed by syn-melt deformation of the shear zone causing a relative strength increase towards the shear zone centre upon crystallisation. The second phase nucleated two parallel shear zones at the edges of the larger ØSZ. There is a lack of evidence to determine if the post-melt deformation of the shear zone by SGR and basal <a> slip is part of the same or a later deformation event. If it is a later deformation event it could be part of the Finnmarkian orogeny, an early Caledonian deformation phase. This would mean crystallised areas of partial melt are not 'dry and strong' if there are significant heterogeneities (e.g. grain size).

[Figure 8 about here.]

Post-melt deformation at the shear zone edges are a similar structure to paired shear zones observed at the mm to cm scale in ductile mid to lower crust, such as the Neves area, Eastern Alps (Mancktelow and Pennacchioni, 2005; Pennacchioni and Mancktelow, 2007) and Fiordland, New Zealand (Smith et al., 2015). The central syn-melt deformation zone of the ØSZ is 500m wide with 100 to 150m wide post-melt shear zones flanking the partial melt shear zone. The ØSZ is 4-5 orders of magnitude wider than those observed by Mancktelow and Pennacchioni (2005); Pennacchioni and Mancktelow (2007) and Smith et al. (2015). We suggest that the ØSZ is a large-scale manifestation of the same mechanisms where paired shear zones flank mm to cm scale strong heterogeneities in the rock. During syn-melt deformation, strain localised towards the centre of the ØSZ where the melt fraction was highest. Upon crystallisation and formation of the paired shear zones flanking the former syn-melt shear zone, strain partitioned to the edges.

In terms of idealised models for shear zone activity and thickness suggested by Fossen and Cavalcante (2017), the ØSZ initially displays 'Type 2' deformation where strain localises to the centre of the shear zone (where the melt fraction is greater). However, once the melt crystallises and strain localises to the edges, the ØSZ represents a 'Type 1' shear zone leaving the central portion strain free and inactive.

The SIP represents a former rift zone where the paragneiss shear zones formed during synintrusive deep crustal shearing (Elvevold et al., 1994; Roberts et al., 2006). Evidence for these shear zones has been observed in present day rifted margins (e.g. Atlantic rifting; Clerc et al., 2015,0) as well as older, former

Iapetus margins (e.g. Kjøll et al., 2019). When considering SIP emplacement alongside the shear zones it suggests the SIP was part of a magma-rich continental rift zone where the paragneiss formed ductile mid crustal shear zones as demonstrated in Figure 8. When this tectonic model is combined with U-Pb age data ($\sim$565 Ma after Roberts et al., 2006) and the microstructural analysis from this study, it indicates partial melting in the ØSZ occurred after emplacement of the SIP gabbro but was short-lived, with deformation contining post-melt to accommodate extension on the Baltica margin.

Conclusions

Coexistence of deformation and melt microstructures suggests a complex geological history for the ØSZ. In contrast to conventional expectations for melt-free shear zones, a reverse grain size distribution is observed with finer grains at the shear zone edges and coarser grains in the centre. In addition, high-temperature, low stress deformation microstructures (GBM, prism <a> slip) are recognised in the shear zone centre, with mid-temperature, high stress deformation microstructures (SGR, basal <a> slip) at the shear zone edges.

We argue that strain localised towards the centre of the shear zone during a regional temperature increase, which ultimately led to partial melting. During the pre-melt phase, the shear zone deformed at high temperatures resulting in grain growth from GBM deformation. During partial melting, melt localised strain during this time and absorbed the majority of the stress. The percolation of melt and formation of melt textures dissect the pre-melt deformation and overprint some of these microstructures. The high temperatures and crystallisation from partial melt promoted further grain growth of already relatively coarse grained restite phases in the shear zone. Once all the melt had crystallised and/or escaped from the system and the temperature decreased, the centre of the shear zone was 'strong' relative to the finer grained margins. As the temperature decreased further, and the stress absorbed by the solid phases increased, the finer grains proved easier to deform and hence strain partitioned to the shear zone boundaries forming the paired shear zones observed today. Unlike partial melt shear zones where melt organisation and pinning of grain growth promotes grain size reduction, grain growth during crystallisation of the ØSZ centre transferred stress to shear zone edges to permit continued deformation and extension of the Baltica margin, suggesting syn-melt shear zones form significant heterogeneities to continue reduce the strength of the crust upon crystallisation.

Melt migration towards the centre of the shear zone ultimately led to strengthening of the shear zone core, with post-crystallisation deformation focusing along shear zone margins.

Acknowledgements

ALL thanks the Timothy Jefferson Field Research fund, part of the Geological Society of London's 2015 research grants, which helped to fund fieldwork in Norway; Andrew Parsons is also thanked for field assistance. AMW is grateful for support from the UK Natural Environment Research Council (NE/K008803/1 and NE/M000044/1).

References

Abdelmalak, M. M., Faleide, J. I., Planke, S., Gernigon, L., Zastrozhnov, D., Shephard, G. E., and Myklebust, R. (2017). The T-Reflection and the Deep Crustal Structure of the Vøring Margin, Offshore mid-Norway. *Tectonics*, 36(11):2497–2523.

Akselsen, J. (1982). Precambrian and Caledonian tectonometamorphic evolution of northeastern Seiland, Finnmark, North Norway. *Norges Geologiske Undersøkelse Bulletin*, 373(1977):45–61.

Austrheim, H. and Boundy, T. M. (1994). Pseudotachylytes Generated During Seismic Faulting and Eclogitization of the Deep Crust. *Science*, 265(5168):82–83.

Brown, M. (2001). Orogeny, migmatites and leucogranites: A review. *Journal of Earth System Science*, 110(4):313–336.

Brown, M. (2007). Crustal melting and melt extraction, ascent and emplacement in orogens: mechanisms and consequences. *Journal of the Geological Society*, 164(4):709–730.

Brown, M., Averkin, Y. A., McLellan, E. L., and Sawyer, E. W. (1995). Melt segregation in migmatites. *Journal of Geophysical Research: Solid Earth*, 100(B8):15655.

Clerc, C., Jolivet, L., and Ringenbach, J.-c. (2015). Ductile extensional shear zones in the lower crust of a passive margin. *Earth and Planetary Science Letters*, 431:1–7.

Clerc, C., Ringenbach, J.-c., Jolivet, L., and Ballard, J.-f. (2018). Rifted margins: Ductile deformation, boudinage, continentward-dipping normal faults and the role of the weak lower crust. *Gondwana Research*, 53:20–40.

Cross, A. J., Prior, D. J., Stipp, M., and Kidder, S. (2017). The recrystallized grain size piezometer for quartz: An EBSD-based calibration. *Geophysical Research Letters*, 44:6667–6674.

Degli Alessandrini, G., Menegon, L., Malaspina, N., Dijkstra, A. H., and Anderson, M. W. (2017). Creep of mafic dykes infiltrated by melt in the lower continental crust (Seiland Igneous Province, Norway). *Lithos*, 274-275:169–187.

Elvevold, S., Reginiussen, H., Krogh, E. J., and Bjørklund, F. (1994). Reworking of deep-seated gabbros and associated contact metamorphism paragneisses in the southeastern part of the Seiland Igneous Province, northern Norway. *Journal of Metamorphic Geology*, 12:539–556.

Evans, B., Renner, J., and Hirth, G. (2001). A few remarks on the kinetics of static grain growth in rocks. *International Journal of Earth Sciences*, 90(1):88–103.

Fossen, H. and Cavalcante, G. C. G. (2017). Shear zones - A review. *Earth-Science Reviews*, 171(May):434–455.

Gleason, G. C. and Tullis, J. (1995). A flow law for dislocation creep of quartz aggregates determined with the molten salt cell. *Tectonophysics*, 247(1-4):1–23.

Guillope, M. and Poirier, J.-P. (1979). Dynamic recrystallisation during creep of single crystalline halite: an experimental study. *Journal of Geophysical Research: Solid Earth*, 84(2):5557–5567.

Hirth, G., Teyssier, C., and Dunlap, W. J. (2001). An evaluation of quartzite flow laws based on comparisons between experimentally and naturally deformed rocks. *International Journal of Earth Sciences*, 90(1):77–87.

Hirth, G. and Tullis, J. (1992). Dislocation creep regimes in quartz aggregates. *Journal of Structural Geology*, 14(2):145–159.

Holness, M. B. and Sawyer, E. W. (2008). On the pseudomorphing of melt-filled pores during the crystallization of migmatites. *Journal of Petrology*, 49(7):1343–1363.

Hull, J. (1988). Thickness-displacement relationships for deformation zones. *Journal of Structural Geology*, 10(4):431–435.

Jurewicz, S. R. and Watson, E. B. (1985). The distribution of partial melt in a granitic system: The application of liquid phase sintering theory. *Geochimica et Cosmochimica Acta*, 49(5):1109–1121.

Karato, S., Paterson, M. S., and Fitz Gerald, J. D. (1986). Rheology of synthetic olivine aggregates: influence of grain size and water. *Journal of Geophysical Research: Solid Earth*, 91(B8):8151–8176.

Karato, S.-i. (2010). Rheology of the deep upper mantle and its implications for the preservation of the continental roots: A review. *Tectonophysics*, 481(1-4):82–98.

Kjøll, H. J., Andersen, T. B., Corfu, F., Labrousse, L., Tegner, C., Abdelmalak, M. M., and Planke, S. (2019). Timing of break-up and thermal evolution of a pre-Caledonian Neoproterozoic exhumed magma-rich rifted margin. *Tectonics*.

Krogh, E. J. and Elvevold, S. (1990). A Precambrian age for an early gabbro-monzonitic intrusive on the Øksfjord peninsula, Seiland Igneous Province, northern Norway. *Norsk Geologisk Tidsskrift*, 70(4):267–273.

Kruhl, J. H. (1996). Prism- and basal-plane parallel subgrain boundaries in quartz: a microstructural geothermobaromether. *Journal of Metamorphic Geology*, 14:581–589.

Labrousse, L., Jolivet, L., Andersen, T. B., Agard, P., and Maluski, H. (2004). Pressure-temperature-time deformation history of the exhumation of ultra-high pressure rocks in the Western Gneiss Region, Norway. *Geological Society of America, Special Papers*, 380:155–183.

Law, R. D., Schmid, S. M., and Wheeler, J. (1990). Simple shear deformation and quartz crystallographic fabrics: a possible natural example from the Torridon area of NW Scotland. *Journal of Structural Geology*, 12(1):29–45.

Lee, A. L., Torvela, T., Lloyd, G. E., and Walker, A. M. (2018). Melt organisation and strain partitioning in the lower crust. *Journal of Structural Geology*, 113:188–199.

Lee, A. L., Walker, A. M., Lloyd, G. E., and Torvela, T. (2017). Modeling the impact of melt on seismic properties during mountain building. *Geochemistry, Geophysics, Geosystems*, 18(3):1090–1110.

Llorens, M.-G., Gomez-Rivas, E., Ganzhorn, A.-C., Griera, A., Steinbach, F., Roessiger, J., Labrousse, L., Walte, N. P., Weikusat, I., and Bons, P. D. (2019). The effect of dynamic recrystallisation on the rheology and microstructures of partially molten rocks. *Journal of Structural Geology*, 118(April 2018):224–235.

Luan, F. C. and Paterson, M. S. (1992). Preparation and deformation of synthetic aggregates of quartz. *Journal of Geophysical Research: Solid Earth*, 97(B1):301–320.

Mancktelow, N. S. and Pennacchioni, G. (2005). The control of precursor brittle fracture and fluid – rock interaction on the development of single and paired ductile shear zones. *Journal of Structural Geology*, 27:645–661.

Means, W. D. (1995). Shear zones and rock history. *Tectonophysics*, 247:157–160.

Menegon, L., Nasipuri, P., Stünitz, H., Behrens, H., and Ravna, E. K. (2011). Dry and strong quartz during deformation of the lower crust in the presence of melt. *Journal of Geophysical Research: Solid Earth*, 116(10):B10410.

Nachlas, W. O. and Hirth, G. (2015). Experimental constraints on the role of dynamic recrystallization on resetting the Ti-in-quartz thermobarometer. *Journal of Geophysical Research: Solid Earth*, 120:8120–8137.

Nixon, R. D., Davis, R. F., Carolina, N., and Carolina, N. (1992). Diffusion-Accommodated Grain Boundary Sliding and Dislocation Glide in the Creep of Sintered Alpha Silicon Carbide. *Journal of the American Ceramic Society*, 75(7):1786–1795.

Olgaard, D. L. and Evans, B. (1988). Grain growth in synthetic marbles with added mica and water. *Contributions to Mineralogy and Petrology*, 100(2):246–260.

Ord, A. and Christie, J. M. (1984). Flow stresses from microstructures in mylonitic quartzites of the Moine Thrust zone, Assynt area, Scotland Geological setting. *Journal of Structural Geology*, 6(6):639–654.

Otani, M. and Wallis, S. (2006). Quartz lattice preferred orientation patterns and static recrystallization: Natural examples from the Ryoke belt, Japan. *Geology*, 34(7):561–564.

Parsons, A. J., Law, R. D., Lloyd, G. E., Phillips, R. J., and Searle, M. P. (2016). Thermo-kinematic evolution of the Annapurna-Dhaulagiri Himalaya, central Nepal: The Composite Orogenic System. *Geochemistry, Geophysics, Geosystems*, 17:1511–1539.

Passchier, C. W. (1982). Pseudotachylyte and the development of ultramylonite bands in the Saint-Barthelemy Massif, French Pyrenees. *Journal of Structural Geology*, 4(1).

Passchier, C. W. and Trouw, R. A. J. (2005). *Microtectonics*. Springer, Berlin, Heidelberg, New York.

Pennacchioni, G. and Cesare, B. (1997). Ductile-brittle transition in pre-Alpine amphibolite facies mylonites during evolution from water-present to water-deficient conditions (Mont Mary nappe, Italian Western Alps). *Journal of Metamorphic Geology*, 15:777–791.

Pennacchioni, G. and Mancktelow, N. S. (2007). Nucleation and initial growth of a shear zone network within compositionally and structurally heterogeneous granitoids under amphibolite facies conditions. *Journal of Structural Geology*, 29:1757–1780.

Poirier, J.-P. (1985). *Creep of crystals: high-temperature deformation processes in metals, ceramics and minerals*. Cambridge University Press.

Ramsay, D. M. and Sturt, B. A. (1986). The contribution of the Finnmarkian orogeny to the framework of the Scandinavian Caledonides. In Fettes, D. J. and Harris, A. L., editors, *Synthesis of the Caledonian rocks of Britain*, pages 221–246. Springer, Dordrecht.

Ramsay, D. M., Sturt, B. A., Jansen, Ø., Andersen, T. B., and Sinha-Roy, S. (1985). The tectonostratigraphy of western Porsangerhalvøya, Finnmark, north Norway. In Gee, D. G. and Sturt, B. A., editors, *The Caledonide Orogen: Scandinavia and related areas*, pages 611–619. John Wiley, Chichester, UK.

Ramsay, J. G. and Graham, R. H. (1970). Strain variation in shear belts. *Canadian Journal of Earth Sciences*, 7(3):786–813.

Reginiussen, H., Ravna, E. K., and Berglund, K. (1995). Mafic dykes from Øksfjord, Seiland Igneous Province, northern Norway: geochemistry and palaeotectonic significance. *Geological Magazine*, 132(6):667–681.

Richter, B., Stünitz, H., and Heilbronner, R. (2016). Stresses and pressures at the quartz-to-coesite phase transformation in shear deformation experiments. *Journal of Geophysical Research: Solid Earth*, 121(11):8015–8033.

Roberts, D. (1973). Geologisk kart over Norge, berggrunnskart. Hammerfest 1: 250 000. *Norges Geologiske Undersøkelse Bulletin*, 61:1–49.

Roberts, D. (1974). Hammerfest: beskrivelse til det 1: 250.000 berggrunnsgeologiske kart. *Norges Geologiske Undersøkelse*, 301:1–66.

Roberts, D. (2003). The Scandinavian Caledonides: Event chronology, palaeogeographic settings and likely modern analogues. *Tectonophysics*, 365(1-4):283–299.

Roberts, R. J., Corfu, F., Torsvik, T. H., Ashwal, L. D., and Ramsay, D. M. (2006). Short-lived mafic magmatism at 560-570 Ma in the northern Norwegian Caledonides: U-Pb zircon ages from the Seiland Igneous Province. *Geological Magazine*, 143:887–903.

Robins, B. and Often, M. (1996). Field Trip Guidebook: The Seiland Igneous Province, North Norway, IGCP Project 336. *Norges Geologiske Undersøkelse Report*, 96(127):1–30.

Rosenberg, C. L. and Handy, M. R. (2005). Experimental deformation of partially melted granite revisited: Implications for the continental crust. *Journal of Metamorphic Geology*, 23(1):19–28.

Sawyer, E. W. (1994). Melt segregation in the continental crust. *Geology*, 22:1019–1022.

Slagstad, T., Melezhik, V. A., Kirkland, C. L., Zwaan, K. B., Roberts, D., Gorokhov, I. M., and Fallick, A. E. (2006). Carbonate isotope chemostratigraphy suggests revisions to the geological history of the West Finnmark Caledonides, northern Norway. *Journal of the Geological Society*, 163(2):277–289.

Smith, J. R., Piazolo, S., Daczko, N. R., and Evans, L. (2015). The effect of pre-tectonic reaction and annealing extent on behaviour during subsequent deformation: insights from paired shear zones in the lower crust of Fiordland, New Zealand. *Journal of Metamorphic Geology*, 33:557–577.

Spear, F. S., Kohn, M. J., and Cheney, J. T. (1999). P -T paths from anatectic pelites. *Contributions to Mineralogy and Petrology*, 134:17–32.

Stephens, M. B. and Gee, D. G. (1989). Terranes and polyphase accretionary history in the Scandinavian Caledonides. *Geological Society of America, Special Papers*, 230:17–30.

Stipp, M., Stünitz, H., Heilbronner, R., and Schmid, S. M. (2002). The eastern Tonale fault zone: a 'natural laboratory' for crystal plastic deformation of quartz over a temperature range from 250 to 700C. *Journal of Structural Geology*, 24:1861–1884.

Stipp, M. and Tullis, J. (2003). The recrystallized grain size piezometer for quartz. *Geophysical Research Letters*, 30(21):1–5.

Sturt, B. A., Pringle, R., and Ramsay, D. M. (1978). The Finnmarkian phase of the Caledonian orogeny. *Journal of Structural Geology*, 135(6):591–610.

Tokle, L., Hirth, G., and Behr, W. M. (2019). Flow laws and fabric transitions in wet quartzite. *Earth and Planetary Science Letters*, 505:152–161.

Twiss, R. J. (1977). Theory and applicability of a recrystallized grain size paleopiezometer. In *Stress in the Earth*, pages 227–244. Birkhäuser, Basel.

Urai, J. L., Means, W. D., and Lister, G. S. (1986). Dynamic recrystallization of minerals. *Mineral and rock deformation: laboratory studies*, 36:161–199.

Vanderhaeghe, O. (2009). Migmatites, granites and orogeny: Flow modes of partially-molten rocks and magmas associated with melt/solid segregation in orogenic belts. *Tectonophysics*, 477(3-4):119–134.

Vitale, S. and Mazzoli, S. (2008). Heterogeneous shear zone evolution: The role of shear strain hardening/softening. *Journal of Structural Geology*, 30(11):1383–1395.

Walte, N. P., Bons, P. D., and Passchier, C. W. (2005). Deformation of melt-bearing systems - Insight from in situ grain-scale analogue experiments. *Journal of Structural Geology*, 27(9):1666–1679.

Walte, N. P., Bons, P. D., Passchier, C. W., and Koehn, D. (2003). Disequilibrium melt distribution during static recrystallization. *Geology*, 31(11):1009–1012.

White, S. (1979). Grain and sub-grain size variations across a mylonite zone. *Contributions to Mineralogy and Petrology*, 70(2):193–202.

Yakymchuk, C. and Brown, M. (2014). Behaviour of zircon and monazite during crustal melting. *Journal of the Geological Society*, 171(4):465–479.

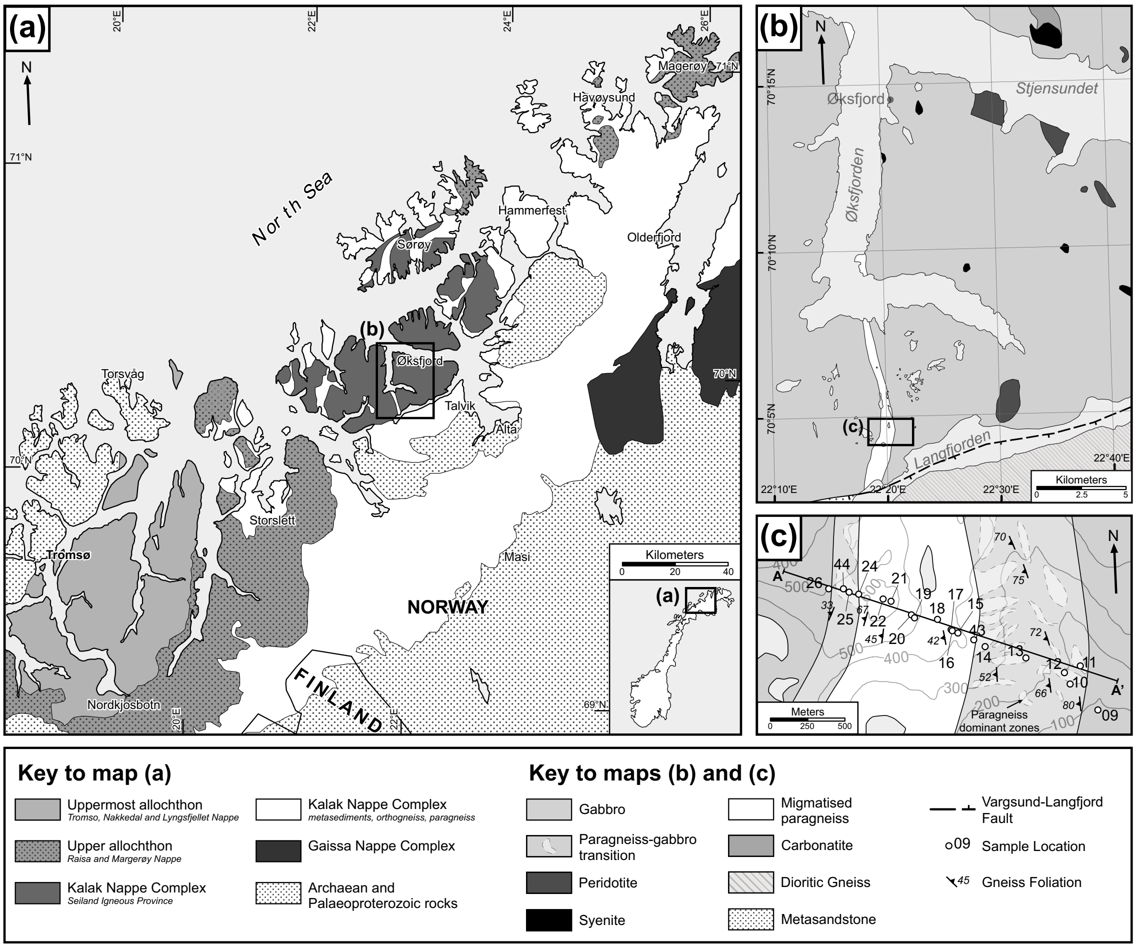

Fig. 1. Geological map of (a) northern Norway and Seiland Igneous Province with inset detail maps of (b) Øksfjord Peninsula in the Seiland Igneous Province and (c) Øksfjord shear zone transect (Geological maps modified from Roberts, 1973; Slagstad et al., 2006).

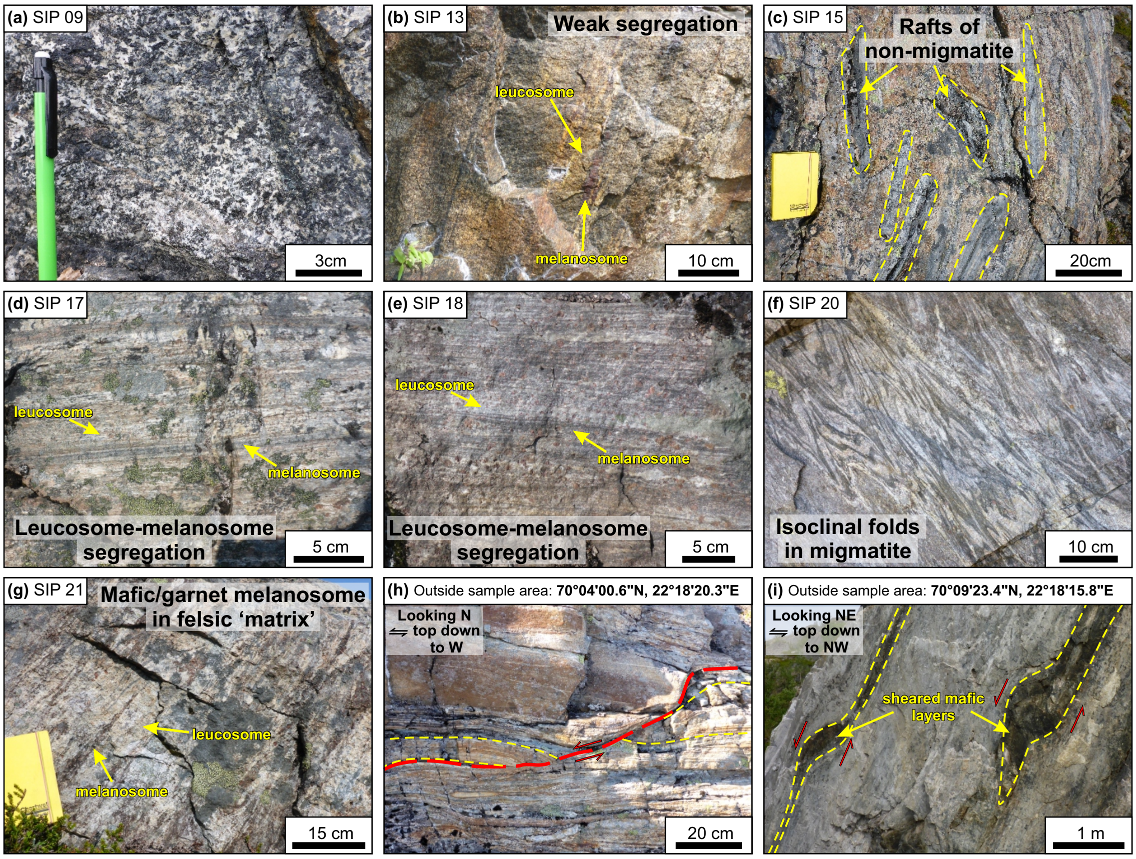

Fig. 2. Outcrop photographs from the ØSZ showing the transition from from localised melt zones within gabbro to highly segregated stromatic migmatites with high temperature mineral assemblages and internal deformation. (a) Gabbro outside transition zone. (b) Transition zone paragneiss on edge of pod with weak leucosome-melanosome segregation. (c) Schollen-type migmatite near the edge of the shear zone boundary; rafts of mesosome within predominantly leucosome. (d) Stromatic migmatized paragneiss. (e) Stromatic segregation of leucosome and melanosome increases in strength towards shear zone centre. (f) Isoclinal folds in stromatic migmatized paragneiss. (g) Migmatized paragneiss with mafic, garnet melanosome layers within a leucratic matrix. (h) Flanking structure with top down to west shearing in paragneiss, outcrop is located outside sample area. (i) Top down to west sheared mafic bands in leucratic paragneiss, outcrop is located outside sample area.

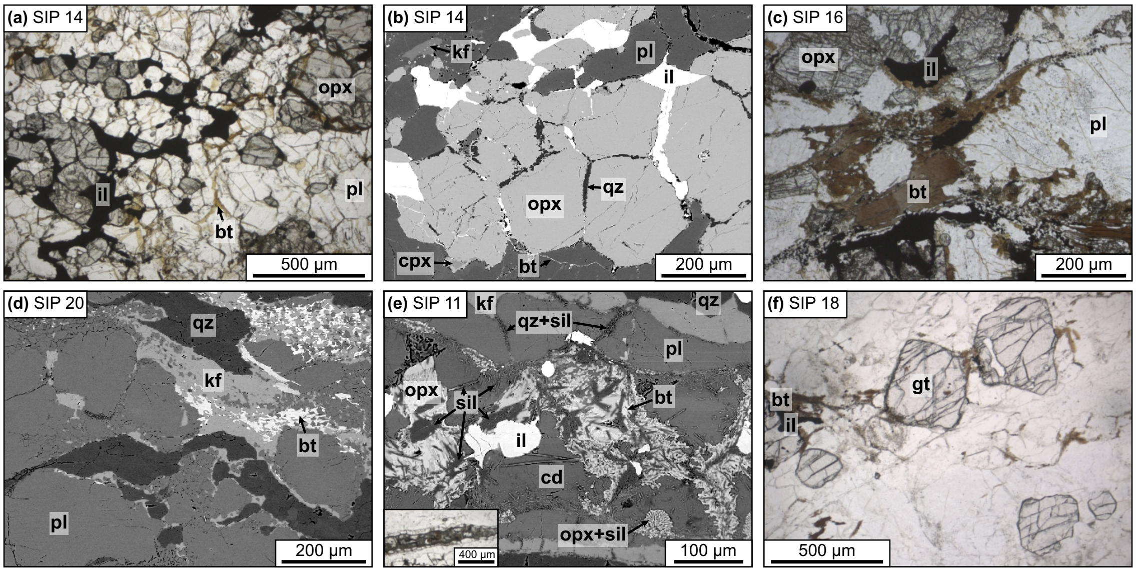

Fig. 3. Melt textures from the ØSZ from thin section photomicrographs (a, c, g) and backscattered electron images (b, d, e). (a-b) Cuspate and interstitial ilmenite, il, melt. (c-d) Biotite, bt, breakdown to K-feldspar, kf, and plagioclase, pl, forming melt at grain boundaries of quartz, qz, and plagioclase. (e) Melt zone within paragneiss, complex textures of orthopyroxene, opx, sillimanite, sil, cordierite, cd, and ilmenite. (f) Peritectic garnets, gt, produced during biotite dehydration melting reactions.

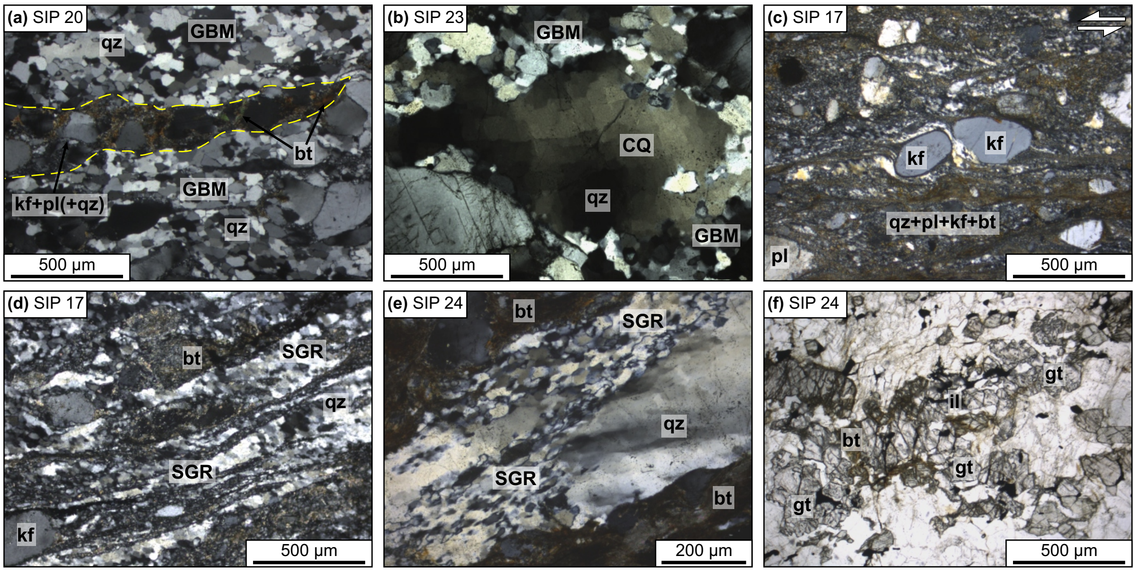

Fig. 4. Thin section photomicrographs of deformation microstructures from the ØSZ. (a) Lobate/serrated grain boundaries of quartz recrystallising by GBM cut by a K-feldspar, plagioclase and biotite melt band highlighted in yellow. (b) Large quartz grain showing chessboard extinction (CQ) with an undulose extinction overprint, smaller grains at edge recrystallised by GBM. (c) Sigmoidal feldspar clasts with sinistral sense of shear. (d) Recrystallisation of quartz ribbons and grains by SGR. (e) Large quartz grain recrystallising by SGR. (f) Retrogressed garnet breaking down to quartz, feldspars and biotite.

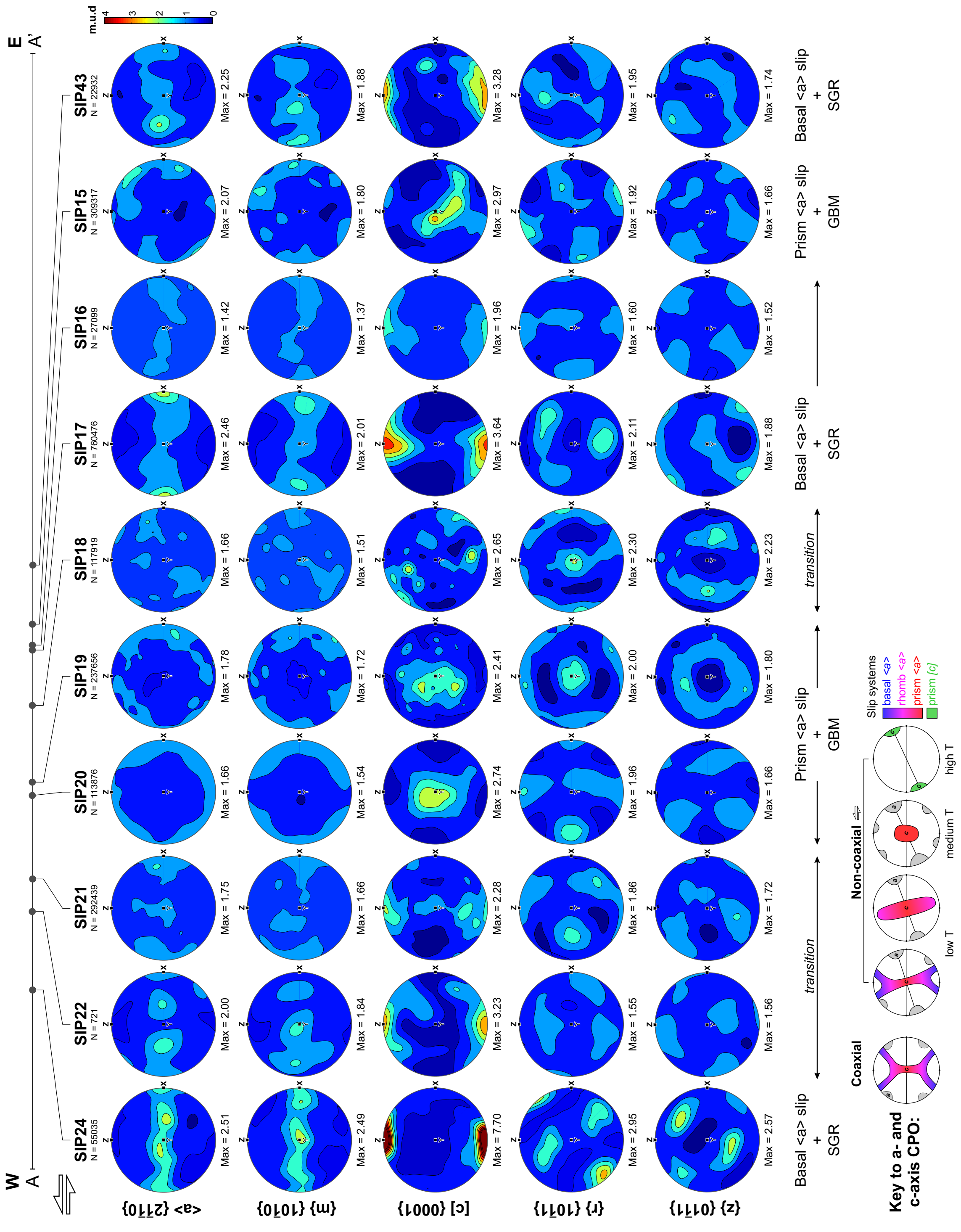

Fig. 5. CPO pole figures for 10 quartz-bearing samples within the ØSZ. Location on section line A-A' is shown above the pole figures and active slip systems and deformation mechanisms are shown below. Beneath the ØSZ CPO is a key to the a- and c-axis CPO development and active slip systems showing temperature dependent CPO development of <a> (grey) and [c] (coloured maxima) during coaxial and non-coaxial dextral shearing (Modified from Passchier and Trouw, 2005; Parsons et al., 2016).

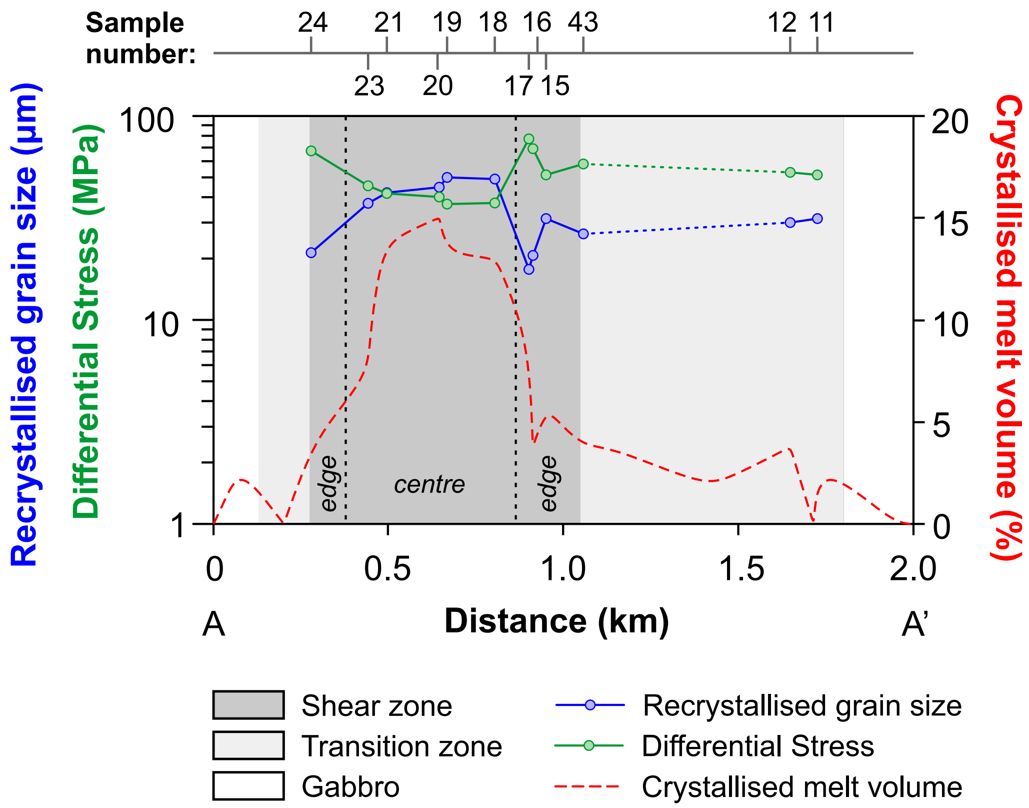

Fig. 6. Recrystallised grain size and palaeopiezometer for quartz bearing samples from the ØSZ. Recrystallised grain size (blue) calculated from EBSD data using GOS; palaeopiezometer (green) relationship after Cross et al. (2017); and melt volume (red) calculated from melt vs. solid image analysis interpretations of photomicrographs.

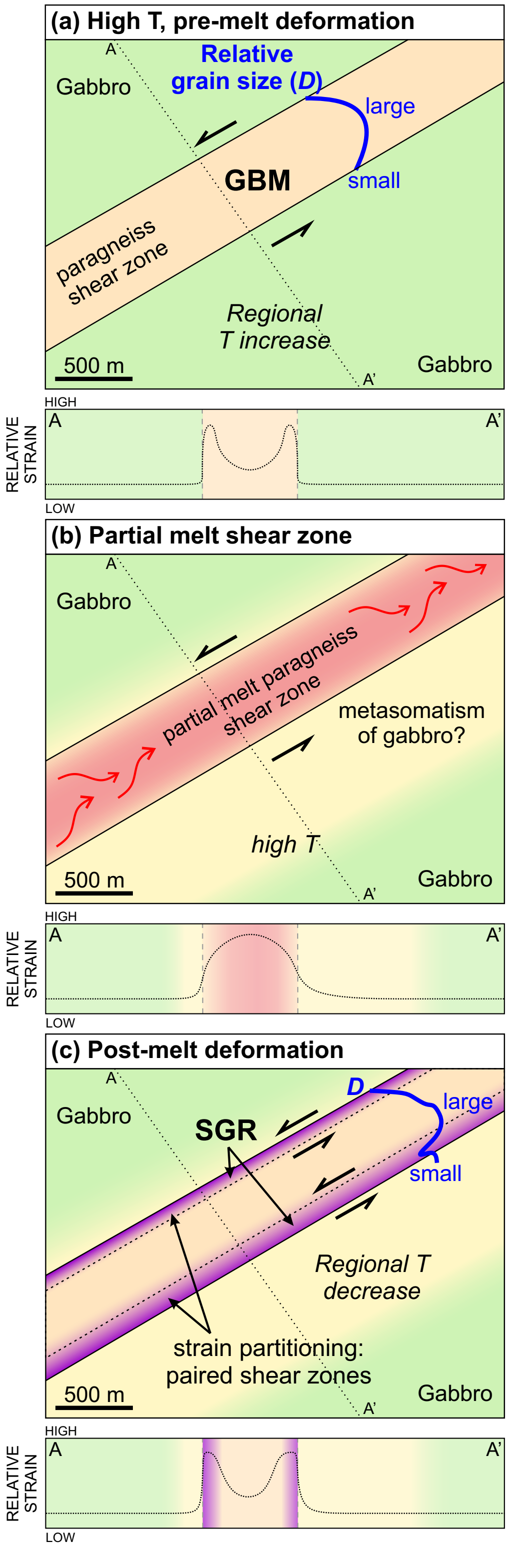

Fig. 7. Schematic diagrams of pre-, syn-, and post-melt shear zones to the ØSZ, relative strain rate is shown beneath each schematic. (a) A 'typical' non-melt shear zone will have a recrystallised grain size (*D*) distribution of large grains at the edges and small grains in the centre where stress and strain rate is greatest, but if it is deforming at high temperatures and GBM is the active deformation mechanism, deformation will result in solid state, static grain growth. Relative strain: low in centre, high at edges. (b) Syn-melt deformation in the ØSZ; higher melt volume towards shear zone centre promotes a grain size increase in crystallisation of peritectic phases, at this stage solid phases do not deform as melt localises the strain. Relative strain: high in centre, low at edges. (c) Crystallisation of shear zone and post-melt deformation; upon regional temperature decrease the shear zone crystallises forming a 'strong' centre, pre-melt GBM deformation and melt-induced grain growth produces a grain size distribution from small to large from edges to centre. Post-melt deformation results in a partitioning of strain to shear zone edges where grain size is smaller, the deformation forms a set of paired shear zones deforming by SGR at lower temperature and higher stress, overprinting evidence for melting at shear zone edges. Relative strain: low in centre, high at edges.

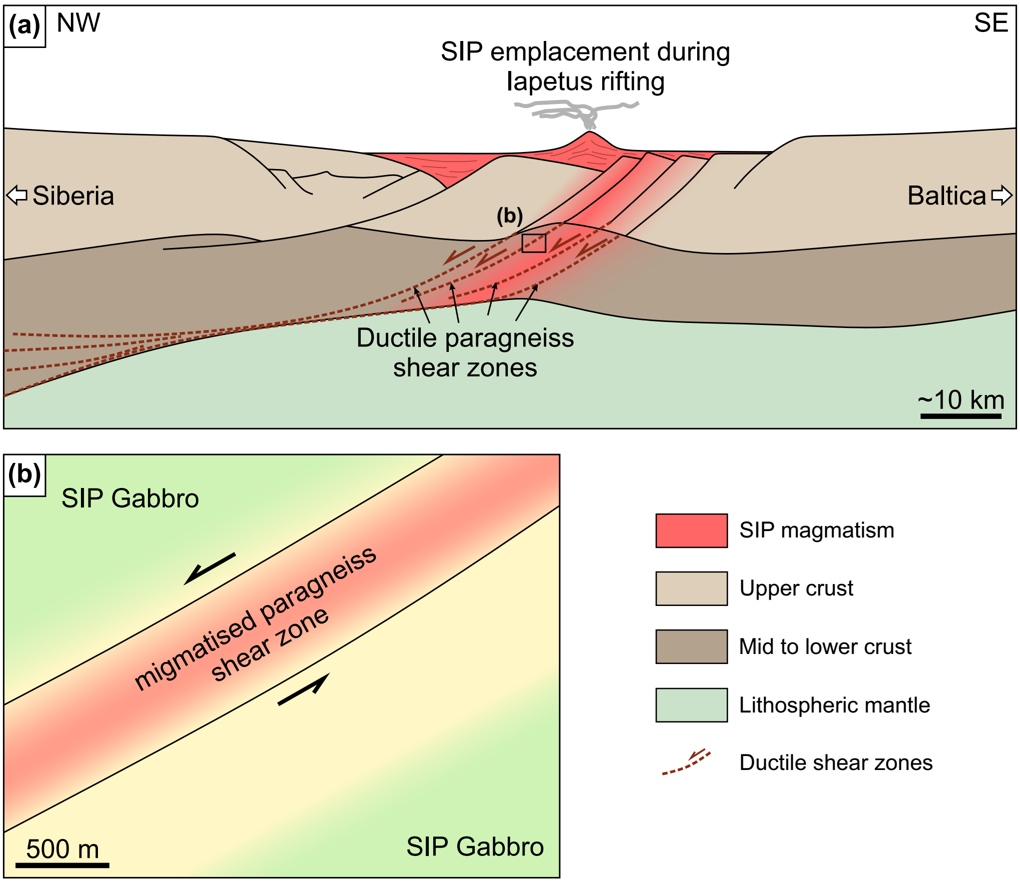

Fig. 8. (a) Tectonic model for SIP emplacement and shear zone development adapted from models by Clerc et al. (2015); Abdelmalak et al. (2017); Kjøll et al. (2019). (b) The ØSZ represents a ductile shear zone within the middle to lower crust.